

Effects of Neutrino Trapping on Thermodynamic Properties of Nuclear “Pasta”

Gentaro Watanabe^a, Kei Iida^{a,b}, Katsuhiko Sato^{a,c}

^a*Department of Physics, University of Tokyo, 7-3-1 Hongo, Bunkyo, Tokyo 113-0033, Japan*

^b*Department of Physics, University of Illinois at Urbana-Champaign, 1110 West Green Street, Urbana, IL 61801-3080, USA*

^c*Research Center for the Early Universe, University of Tokyo, 7-3-1 Hongo, Bunkyo, Tokyo 113-0033, Japan*

November 1, 2018

Abstract

Geometrical structure of matter at subnuclear densities is investigated in the presence of a degenerate gas of neutrinos as encountered in stellar collapse. The crystalline phases with spherical, cylindrical and planar nuclei as well as with spherical and cylindrical nuclear bubbles are considered by using a compressible liquid-drop model. This model allows for uncertainties in the lepton fraction Y_L in addition to those in the nuclear surface tension E_{surf} and in the proton chemical potential in bulk neutron matter $\mu_p^{(0)}$. The phase diagrams obtained at zero temperature show that only the phases with rod-like and slab-like nuclei occur at typical values of Y_L , E_{surf} and $\mu_p^{(0)}$, whereas the bubble phases, especially with spherical bubbles, are at best expected at hypothetically low values of Y_L and/or E_{surf} . For the rod-like and slab-like nuclei, thermally induced displacements are calculated from their respective elastic constants. It is found that at temperatures appropriate to supernova cores, thermal fluctuations would destroy the layered lattice of slab-like nuclei almost independently of the nuclear models and of the degree of the neutrino degeneracy.

PACS : 26.50.+x; 97.60.Bw

Keywords : Dense matter; Ground state; Thermal fluctuations; Stellar collapse

1 Introduction

To clarify the mechanism of collapse-driven supernovae (see, e.g., Refs. [1, 2] for review) necessitates understanding of the properties of matter under extreme conditions characterized by high densities and temperatures as well as of its interactions with electron neutrinos, which are produced by electron capture processes on the nuclei present during the collapse of an iron core of a massive star. Diffusion of the neutrinos thus produced is controlled by their coherent scattering off the nuclei via neutral-current weak interactions [3, 4]. It is generally accepted that at densities above $\sim 10^{12} \text{ g cm}^{-3}$, where the dynamical time scale of the collapse is small compared with the diffusion time scale, these neutrinos are trapped, forming an ultrarelativistic and degenerate Fermi gas. This plays a role in establishing β equilibrium in the system¹ and, until the core ceases to collapse and rebounds, in increasing the system temperature T up to order or greater than 10 MeV. The density region in which such a trapping occurs and the lepton fraction, i.e., the number of the leptons of electron flavor present per nucleon locally in this region:

$$Y_L = \frac{n_e + n_\nu}{n_b} , \quad (1)$$

where n_b , n_e and n_ν are the nucleon, electron and electron-neutrino number densities, respectively, depend on the rates of the electron capture and of the neutrino scattering. These rates are in turn affected by changes in the states of supernova matter such as changes in the nuclear composition and a melting transition from the phase with the nuclei to the phase of uniform nuclear matter.

¹ Hereafter, the corresponding β equilibrated material is referred to as supernova matter.

At subnuclear densities and at temperatures below the critical temperature of order 10 MeV, nuclear matter is separated into a high-density liquid part, usually characterized by roughly spherical nuclei, and a low-density gas part, composed mostly of neutrons. When the density is close to the saturation density of symmetric nuclear matter, $\rho_s \approx 2.7 \times 10^{14}$ g cm⁻³, the system is expected to have rod-like and slab-like nuclei as well as rod-like and roughly spherical bubbles, as originally indicated by Ravenhall et al. [5] and Hashimoto et al. [6] using a liquid drop model in the zero-temperature approximation. These earliest investigations show that such non-spherical nuclei and bubbles, forming a Coulomb lattice, arise from a delicate balance between the interfacial energy and the electrostatic energy including the lattice energy. With increasing density, a bcc lattice of spherical nuclei changes into a two-dimensional triangular lattice of rod-like nuclei and then into a one-dimensional layered lattice of slab-like nuclei, until the liquid part and the gas part begin to be replaced by each other. After further transformations to a two-dimensional triangular lattice of cylindrical bubbles and then to a bcc lattice of spherical bubbles, the system turns into uniform nuclear matter. This behavior was confirmed by Lassaut et al. [7] in their three-dimensional Thomas-Fermi calculations at finite Y_L and T relevant to stellar collapse. Those kinds of non-spherical nuclei and of bubbles are often referred to as nuclear “pasta” since they are similar in shape to spaghetti, lasagna, etc.

The presence of non-spherical nuclei and of bubbles is expected to have consequence to the hydrodynamics and neutrino transport in supernova cores; these are ingredients of a simulation study of stellar collapse, bounce and explosion (for recent progress in this study, see, e.g., Ref. [8]). Let us first note that the neutrino wavelengths, typically of

order 20 fm, are comparable to or even greater than the internuclear spacing, leading to diffractive effects on the neutrino elastic scattering off such a periodic spatial structure of nuclear matter [5]. These effects, induced by the internuclear Coulombic correlations, would act to reduce the scattering rates and hence the lepton fraction Y_L . For the bcc lattice of spherical nuclei, such a reduction was examined by Horowitz [9] by calculating the associated static structure factor. As clarified by Bruenn and Mezzacappa [10] in their numerical calculations of stellar collapse, however, the resultant window that allows low-energy neutrinos to diffuse away from the core during its collapse is too narrow to drastically suppress the degree of the neutrino degeneracy. It is also noteworthy that non-spherical nuclei and bubbles are elongated in specific direction. In such direction, the neutrino scattering processes are no longer coherent, in contrast to the case of roughly spherical nuclei whose finiteness in any direction yields constructive interference in the scattering. The last point to be mentioned is that the changes in the nuclear shape are accompanied by discontinuities in the adiabatic index, denoting how hard the equation of state of the material is. As Lassaut et al. [7] suggested, these discontinuities may influence the core hydrodynamics during the initial phase of the collapse.

For neutron star matter, which has vanishing neutrino degeneracy, we examined the density region in which the phases with non-spherical nuclei and with bubbles are preferred over the bcc phase of spherical nuclei and the homogeneous phase by generalizing a compressible liquid-drop model advanced by Baym, Bethe and Pethick [13] (hereafter BBP) so as to incorporate uncertainties in the nuclear surface tension E_{surf} and the proton chemical potential $\mu_p^{(0)}$ in the dripped neutron gas [11]. We found that as E_{surf}

decreases or $\mu_p^{(0)}$ increases, such a density region is enlarged appreciably. Fortunately, those uncertainties are of less importance to supernova matter at subnuclear densities, which will be studied in the present paper. This is because after the onset of the neutrino trapping, the resultant neutrino degeneracy keeps the denser part of nuclear matter stable against further neutronization; not only does the proton fraction x in this part remain typically of order 0.3, not far from the regime accessible to experiment, but also the dripped nucleon gas, arising mainly from thermal effects, is too low for the values of $\mu_p^{(0)}$ to make any essential difference in the density region occupied by nuclear “pasta”. To be taken into account in analyzing supernova matter, in addition to the nuclear model dependence of the stability of the “pasta” phases, is its dependence on the trapped lepton fraction Y_L . The values of Y_L , depending on the sizes and shapes of the denser part which produces, scatters and absorbs electron neutrinos via weak interactions, exert feedback on the condition for the stability of the “pasta” phases. Note, for example, that with increasing Y_L , the melting density ρ_m approaches ρ_s . This is due to the tendency [12] that as the denser part is at larger neutron excess, the saturation density is lowered. By allowing for uncertainties in Y_L coming partly from such a feedback effect, we set a range of Y_L as $0.2 \leq Y_L \leq 0.4$, rather wider than the usually adopted values ranging 0.3–0.38 (see Refs. [1, 2] and references therein). The equilibrium phase diagrams of zero-temperature supernova matter are drawn for this range of Y_L ; we thus find that at typical values of E_{surf} , $\mu_p^{(0)}$ and Y_L , the phases with rod-like and slab-like nuclei lie between the usual bcc phase and the uniform phase, as in the case of neutron star matter [11].

For these two “pasta” phases, we evaluate thermally induced displacements of the

nuclei from their elastic constants, which were described by Pethick and Potekhin [14] in terms of the interfacial and electrostatic energies. They noted that the low-dimensional spatial order exhibited by the phases with cylindrical and planar nuclei is analogous to that of the liquid crystals, i.e., columnar phases and smectics A, respectively. According to our previous analysis of neutron star matter [11], thermal fluctuations may melt the layered lattice of planar nuclei rather than the triangular lattice of cylindrical nuclei at temperatures appropriate to matter in neutron star crusts. In the case of supernova cores of interest here, as we shall see, not only the temperature scale but also the elastic constants are considerably large as compared with the case of neutron star crusts. The temperatures and elastic constants thus increased play a role in enhancing and suppressing the fluctuational displacements, respectively. The resultant rivalry between these two roles is finally examined.

In Section 2, a compressible liquid-drop model for nuclei and bubbles, together with the associated equilibrium conditions, is designed to describe zero-temperature matter at subnuclear densities and various lepton fractions. In Section 3 we therefrom derive the equilibrium phase diagrams for changes in the nuclear conformation. Properties of such conformation changes are discussed in Section 4. In Section 5 we estimate displacements of rod-like and slab-like nuclei at finite temperatures. Section 6 is devoted to conclusions.

2 Model for supernova matter at subnuclear densities

In this section, we construct the free energy of supernova matter for densities near the melting density ρ_m , and write down the conditions for its equilibrium. We concentrate on the influence of the lepton fraction Y_L on the free energy. Since the finite-temperature effects on the free energy, i.e., nuclear and electronic excitations, nucleon evaporation from the denser part of nuclear matter, multiple shapes and sizes of this part, etc., are of less importance, the temperature T is taken to be zero. All we bear in mind is thus to combine the BBP-type compressible liquid-drop model used by us [11] for the description of zero-temperature, inhomogeneous nuclear matter embedded in a sea of electrons with the energy contribution of electron neutrinos. At $T = 0$, the less dense part of nuclear matter is composed entirely of the neutrons dripped out of the denser part.

Following Ref. [11], we consider five phases characterized by the shapes of the denser part of nuclear matter, i.e., sphere, cylinder, slab, cylindrical hole and spherical hole, respectively; each phase is composed of a single species of nucleus or bubble at a given baryon density n_b and lepton fraction Y_L . The Wigner-Seitz approximation is adopted in describing the energy of the respective Coulomb lattice: A cell in the bcc lattice, including a spherical nucleus or bubble of radius r_N , is replaced by a spherical Wigner-Seitz cell having the same center and radius r_c ; a cell in the two-dimensional triangular lattice, including a cylindrical nucleus or bubble having an infinitely long axis and a circular section of radius r_N , is replaced by a cylindrical Wigner-Seitz cell having the same axis and a circular section of radius r_c ; a cell in the one-dimensional layered lattice, including

a planar nucleus with width $2r_N$, is equivalent to a planar Wigner-Seitz cell having the same central plane and width $2r_c$. The values of r_c for these phases are chosen so that each Wigner-Seitz cell may have zero net charge.

2.1 Energy of matter

Let us now regard each species of leptons (nucleons) as uniformly distributed everywhere in the system (inside and outside the nuclei or bubbles), and write down the total energy density E_{tot} of the system as

$$E_{\text{tot}} = \begin{cases} w_N + w_L + (1 - u)E_n(n_n) + E_e(n_e) + E_\nu(n_\nu) & \text{(nuclei) ,} \\ w_N + w_L + uE_n(n_n) + E_e(n_e) + E_\nu(n_\nu) & \text{(bubbles) .} \end{cases} \quad (2)$$

Here, w_N is the energy of the nuclear matter region (the region containing protons) in a cell as divided by the cell volume; w_L is the lattice energy per unit volume as given for the nuclei or bubbles having nonzero r_N ; n_n is the number density of neutrons outside the nuclei or inside the bubbles; E_n , E_e and E_ν are the energy densities of the neutron matter, of the electron gas and of the neutrino gas, respectively; u is the volume fraction occupied by the nuclei or bubbles.

In Eq. (2), the expressions for w_N , w_L , E_n and E_e are given by Eqs. (3), (8), (10) and (11) in Ref. [11]. A new component, the neutrino energy density, is expressed in the form of an ideal ultrarelativistic Fermi gas:

$$E_\nu(n_\nu) = \frac{3}{4}n_\nu\hbar k_\nu c, \quad (3)$$

where $k_\nu = (6\pi^2n_\nu)^{\frac{1}{3}}$ is the neutrino Fermi wave number. Recall that the energy of the nuclear matter region is written in the form of a compressible liquid-drop model as (Eq.

(3) in Ref. [11])

$$w_N(n, x, n_n, r_N, r_c, d) = \begin{cases} un[(1-x)m_n + xm_p]c^2 + unW(k, x) \\ \quad + w_{\text{surf}}(n, x, n_n, r_N, u, d) + w_C(n, x, r_N, u, d) & \text{(nuclei) ,} \\ (1-u)n[(1-x)m_n + xm_p]c^2 + (1-u)nW(k, x) \\ \quad + w_{\text{surf}}(n, x, n_n, r_N, u, d) + w_C(n, x, r_N, u, d) & \text{(bubbles) ,} \end{cases} \quad (4)$$

where m_n (m_p) is the neutron (proton) rest mass; n is the nucleon number density in the nuclear matter region; $W(k, x)$ is the energy per nucleon for uniform nuclear matter of nucleon Fermi wave number $k = (3\pi^2 n/2)^{1/3}$ and proton fraction x ; w_{surf} is the nuclear surface energy per unit volume; w_C is the self Coulomb energy (per unit volume) of protons contained in a cell; d is the dimensionality defined as $d = 1$ for slabs, $d = 2$ for cylinders and $d = 3$ for spheres. This expression for w_N includes three parameters C_1 , C_2 and C_3 , associated with uncertainties in the proton chemical potential $\mu_p^{(0)}$ in pure neutron matter as contained in $W(k, x)$ and those in the nuclear surface tension $E_{\text{surf}} (= r_N w_{\text{surf}}/ud)$. C_1 determines the magnitude of $\mu_p^{(0)}$ (not including the rest mass) as (Eq. (4) in Ref. [11])

$$\mu_p^{(0)} = -C_1 n_n^{2/3} . \quad (5)$$

We basically set $C_1 = 400 \text{ MeV fm}^2$; this case is consistent with the generally accepted behavior among recent literature as exhibited in Fig. 1 of Ref. [11]. As the case may be, $C_1 = 300, 500, 600 \text{ MeV fm}^2$ will be also taken for the sake of comparison. The other two parameters C_2 and C_3 are defined as (Eq. (6) in [11])

$$E_{\text{surf}} = C_2 \tanh\left(\frac{C_3}{\mu_n^{(0)}}\right) E_{\text{surf}}^{\text{BBP}} , \quad (6)$$

where $\mu_n^{(0)} = \partial E_n / \partial n_n - m_n c^2$ is the neutron chemical potential in the neutron gas (not including the rest mass), and $E_{\text{surf}}^{\text{BBP}}$ is the BBP-type surface tension (Eq. (7) in Ref. [11]).

As shown in Ref. [11] for the ground-state matter with $n_\nu = 0$ and $C_1 = 300, 400, 500, 600$ MeV fm², to set $C_2 = 1.0$ and $C_3 = 3.5$ MeV well reproduces the Hartree-Fock (HF) results obtained by Ravenhall, Bennett and Pethick [15] (hereafter denoted by RBP) using a Skyrme interaction. It is important to examine whether or not this tendency persists for the ground-state supernova matter; in this case, the proton fraction x of interest is considerably large relative to the case of $n_\nu = 0$ in which it is confined to $x < 0.2$. When we still set $C_2 = 1.0$ and $C_3 = 3.5$ MeV, as can be seen from Fig. 1, the surface tension calculated from the equilibrium conditions to be described in Subsection 2.2 agrees fairly well with the RBP results for $C_1 = 400$ MeV fm² and $Y_L = 0.2, 0.3, 0.4$.² Such agreement has been confirmed also for $C_1 = 300, 500, 600$ MeV fm² and $Y_L = 0.2, 0.3, 0.4$. In the present work, we thus give C_3 a fixed value, 3.5 MeV, and C_2 a range of values including unity, 0.01–3.

2.2 Equilibrium conditions

Zero-temperature supernova matter with nuclei or bubbles of given shape, in its equilibrium, fulfills the conditions for stability of the nuclear matter region against change in the size, neutron drip, β -decay and pressurization, as in the case of neutron star matter (see Section 2.2 in Ref. [11]). These conditions come from minimization of the energy density E_{tot} with respect to five variables n , x , n_n , r_N and u at fixed lepton fraction Y_L given by Eq. (1) and baryon density n_b given by

$$n_b = \begin{cases} un + (1 - u)n_n & \text{(nuclei) ,} \\ (1 - u)n + un_n & \text{(bubbles) ,} \end{cases} \quad (7)$$

²At fixed Y_L and for densities of interest here, the proton fraction x is limited to a rather small range exhibited in Fig. 1.

as well as under charge neutrality,

$$n_e = \begin{cases} xnu & \text{(nuclei) ,} \\ xn(1 - u) & \text{(bubbles) .} \end{cases} \quad (8)$$

The resultant expressions for the size, drip and pressure equilibria are the same as those given for neutron star matter (see Eqs. (14), (15) and (21) in Ref. [11]). Only the β -equilibrium condition (Eq. (18) in Ref. [11]) is modified by the neutrino degeneracy; it now reads

$$\mu_e - \mu_\nu - (m_n - m_p)c^2 = \mu_n^{(N)} - \mu_p^{(N)} , \quad (9)$$

where

$$\mu_\nu = \hbar k_\nu c \quad (10)$$

is the neutrino chemical potential; μ_e , $\mu_n^{(N)}$ and $\mu_p^{(N)}$ are the electron chemical potential, the neutron chemical potential in the nuclear matter region and the proton chemical potential in the nuclear matter region, respectively (see Eqs. (19), (16) and (20) in Ref. [11]).

At given n_b , Y_L and nuclear shape, we have calculated the minimum value of E_{tot} for electrically neutral supernova matter. Such calculations begin with elimination of μ_ν from condition (9) with the help of Eqs. (1) and (10), leading to a cubic equation for $\mu_e^{\frac{1}{3}}$. The solution for μ_e can then be written in terms of n , x , n_n and r_N by using the Cardan's formula. For the rest of the process that allows us to find the equilibrium values of n , x , n_n , r_N and r_c and thus the minimum value of E_{tot} , we can follow a line of argument of Ref. [11].

At the same n_b and Y_L , the energy density of uniform nuclear matter in β -equilibrium with leptons has also been evaluated. The total energy density of this uniform system is

written as

$$E_{\text{tot}} = nW(k, x) + n[(1 - x)m_n + xm_p]c^2 + E_e(n_e) + E_\nu(n_\nu) , \quad (11)$$

where the presence of muons is ignored. We then minimize E_{tot} with respect to x at fixed baryon density $n_b (= n)$ and lepton fraction Y_L as well as subject to charge neutrality,

$$n_e = xn . \quad (12)$$

The resultant β -equilibrium condition, given by

$$\frac{\partial W(k, x)}{\partial x} = -\mu_e + \mu_\nu + (m_n - m_p)c^2 , \quad (13)$$

leads to the optimal value of x and hence of E_{tot} . By comparing this value of E_{tot} with the values obtained for the five crystalline phases, we have determined the phase giving the smallest energy density at various values of n_b , Y_L , C_1 and C_2 , and thereby drawn the phase diagrams for the ground-state supernova matter, as plotted in Figs. 2 and 3.

3 Phase diagrams

Let us first examine the $\mu_p^{(0)}$ and E_{surf} dependence of the density region of each phase; such dependence can be typically seen from Fig. 2 that exhibits the phase diagram drawn at $Y_L = 0.3$ and $C_1 = 300, 400, 600 \text{ MeV fm}^2$ over the n_b versus C_2 plane. We have thus confirmed the feature as mentioned in Section 1 that the density region where neither the usual bcc phase nor the uniform phase is stable is almost independent of $\mu_p^{(0)}$ because of negligibly small n_n . We remark in passing that the melting density ρ_m increases with increasing C_1 (lowering $\mu_p^{(0)}$), in contrast to the case of neutron star matter (see Fig.

3 in Ref. [11]). This is because such a change in $\mu_p^{(0)}$ helps the nuclear matter region keep the protons within itself, rather than the neutron gas region share the protons. The E_{surf} dependence, on the other hand, is essentially the same as that obtained for neutron star matter: Not only is the density region occupied by nuclear “pasta” reduced with increasing C_2 , but also the sequence of the nuclear shape for the lower E_{surf} ($C_2 \lesssim 0.3$), i.e., sphere \rightarrow cylinder \rightarrow slab \rightarrow cylindrical hole \rightarrow spherical hole \rightarrow uniform matter (with increasing n_b), changes into sphere \rightarrow cylinder \rightarrow slab \rightarrow uniform matter for the typical E_{surf} ($C_2 \simeq 1.0$). However, it is to be recalled that uncertainties accompanying C_2 are smaller for supernova matter than for neutron star matter (see Section 1).

We proceed to consider the Y_L dependence of the phase diagrams by observing Fig. 3 drawn for $Y_L = 0.2, 0.25, 0.3, 0.4$ and for $C_1 = 400 \text{ MeV fm}^2$. For these values of Y_L , within the typical E_{surf} region ($C_2 \simeq 1.0$), the phase with slab-like nuclei dissolves into uniform matter without undergoing a transition to the phase with cylindrical or spherical bubbles. The most viable situation in which at least one of the bubble phases is energetically favored for a finite range of density is expected in a rather hypothetical parameter region, $Y_L \simeq 0.2$ and $C_2 \simeq 0.7$. It is interesting to note that as Y_L increases, the melting density ρ_m goes up and becomes close to ρ_s . As mentioned in Section 1, this is due to the proton fraction dependence of the saturation density; for details, see Fig. 1 in Ref. [16] that shows the BBP model for the energy of bulk nuclear matter underlying $W(k, x)$ used here. We also find that the density region occupied by nuclear “pasta” is considerably larger than that displayed by Fig. 3 in Ref. [11] for neutron star matter having a lepton fraction of order 0.03 and a surface tension of order 0.1 MeV fm^{-2} . This

is because such a density region is controlled by the tendency towards reduction in the total surface area, which is in turn determined by E_{surf} and hence by Y_L (see Fig. 1). This tendency communicates with the fact that for supernova matter, the energy difference between two successive phases is generally of order 1-10 keV per nucleon (see Fig. 4), an order of magnitude larger than that for neutron star matter (see Fig. 4 in Ref. [11]).

We conclude this section by asking why the bubble phases do not appear in the equilibrium phase diagrams for our typical nuclear model ($C_1 = 400 \text{ MeV fm}^2$ and $C_2 = 1.0$) in contrast with the results obtained by Lassaut et al. [7] in their three-dimensional Thomas-Fermi calculations using a Skyrme nucleon-nucleon interaction. As expected from a simple liquid-drop argument of the electrostatic and interfacial effects ignoring the bulk energy [6], they found that all the phases with non-spherical nuclei and with bubbles occur for a finite range of pressure (or density). We ascribe this contrast primarily to the difference in the adopted properties of bulk nuclear matter at a proton fraction of about 0.3; description of these properties relies on interpolation between the fairly-well-determined properties of pure neutron matter and symmetric nuclear matter. This ascription is supported by the speculation that the role of curvature corrections in stabilizing the phases with bubbles relative to the phases with nuclei, which was allowed for in Ref. [7] but has been disregarded in the present work, is not sufficient to cause the bubble phases to appear in the vicinity of $C_2 = 1.0$ on the phase diagrams. Such insufficiency can be viewed from Fig. 5, in which the curvature energy gain per nucleon for spherical bubbles over for planar nuclei and the difference in energy per nucleon between the phases with spherical bubbles and with planar nuclei have been compared for $Y_L = 0.3$, $C_1 = 400 \text{ MeV fm}^2$ and

$C_2 = 1.0$.³ The curvature energy for given conformation is expressed per nucleon as

$$W_{\text{curv}} = \begin{cases} \frac{d(d-1)u\omega_c}{n_b r_N^2} & \text{(nuclei) ,} \\ -\frac{d(d-1)u\omega_c}{n_b r_N^2} & \text{(bubbles) ,} \end{cases} \quad (14)$$

where ω_c is the curvature thermodynamic potential per unit length. We have set the values of ω_c , which have yet to be determined well even at proton fractions near $x = 0.5$, as $\omega_c = 0.1, 0.2, 0.5$ MeV fm⁻¹ by reference to the estimates, $\sim 0.1\text{--}0.2$ MeV fm⁻¹ at $x \sim 0.3$, made by Kolehmainen et al. [17] in the Thomas-Fermi theory with Skyrme interactions. Figure 5 indicates that for the typical parameter set leading to $x \sim 0.3$, the value of ω_c required by the presence of the bubble phases is at least ~ 0.5 MeV fm⁻¹, considerably larger than the estimates referred to. For $\omega_c \sim 0.1\text{--}0.2$ MeV fm⁻¹, all the curvature corrections contribute to the vicinity of $C_2 = 1.0$ on the phase diagrams is to lower the transition density from sphere to cylinder and that from cylinder to slab by several tens percent and to accordingly enlarge the density region surrounded by the bcc phase and the uniform phase.

4 Properties of phase transitions

At a pressure at which the transition between one nuclear shape and another occurs, various quantities such as n_b , r_c , r_N , n , x and n_n are more or less discontinuous because of the dependence of the interfacial and electrostatic energies on the dimensionality d

³ Note that for this parameter set and at densities close to the melting point ρ_m , the phase with cylindrical bubbles is less favorable than that with spherical bubbles even in the absence of the curvature corrections which lower the energy for the spherical-bubble phase further than that for the cylindrical-bubble phase.

(see Eqs. (5) and (8) in Ref. [11]). As can be derived from Fig. 4 by implementing the double-tangent constructions denoting the coexistence of the two neighbouring phases, the discontinuity in n_b amounts to of order 1%. Due to such a weak first-order nature of the transition, the transition point, properly characterized by a constant pressure, is well described by a constant density determined by the comparison between the total energy densities for the respective phases.

Let us then examine the changes in the sizes of the nucleus or bubble and of the Wigner-Seitz cell, r_N and r_c , associated with the structural transitions. In Fig. 6 we have plotted the values of r_N and r_c evaluated as functions of n_b for $Y_L = 0.3$, $C_1 = 400 \text{ MeV fm}^2$ and $C_2 = 0.01, 1.0, 2.5$. Discontinuities in r_N and r_c at the transition points have been thus clarified. In the case of $C_2 = 0.01$ in which all the five crystalline phases appear, we observe the same dimensionality dependence of r_c as observed for neutron star matter (see Fig. 5 in Ref. [11]), i.e., it is largest for $d = 3$ (spheres and cylindrical holes) and smallest for $d = 1$ (slabs).

We finally address the question of how the neutron densities outside and inside the nuclear matter region change as the system melts into uniform nuclear matter. Comparison of these densities with the one for the uniform phase has been made in Fig. 7 for $Y_L=0.3$, $C_1=400 \text{ MeV fm}^2$ and $C_2 = 0.01, 0.1, 1.0, 2.5$. We can observe from this figure that for densities up to the melting point, the density of the dripped neutron gas remains negligibly small compared with the neutron density inside the nuclear matter region. This behavior, which stems from the neutrino trapping (see Section 1) and manifests itself for the other values of Y_L and C_1 , is consistent with the results obtained by Ogasawara and

Sato [18] in their Thomas-Fermi calculations at various values of Y_L and zero temperature. We also find from the comparison of Fig. 7 with Fig. 6 in Ref. [11] that the difference in the neutron density profiles between the crystalline and uniform phases at the melting point is remarkable in contrast with the case of neutron star matter, in which the neutron density profile is fairly levelled just below the melting point. In supernova matter, in which neighbouring nuclei (or bubbles) appear to touch and fuse each other at the melting point, neutrino elastic scattering off nuclear “pasta” is thus expected to take effect until it becomes uniform.

5 Thermal fluctuations

Given occurrence of the phases with rod-like and slab-like nuclei as expected for typical values of E_{surf} and Y_L from the zero-temperature phase diagrams exhibited in the previous section, we turn to the estimates of thermally induced displacements of these nuclei from their equilibrium positions. In making such estimates, we utilize the expressions for such displacements that were written in Ref. [11] on the basis of the elastic constants [14] controlling small deformation of the nuclei. For the layered lattice of slab-like nuclei, the mean square of the displacement v of layers in their normal direction reads (Eq. (36) in Ref. [11])

$$\langle |v|^2 \rangle \simeq \frac{k_B T}{4\pi\sqrt{BK_1}} \ln\left(\frac{L}{a}\right), \quad (15)$$

where k_B is the Boltzmann constant, $a = 2r_c$ is the layer spacing, B and K_1 are the elastic constants given by Eqs. (28) and (29) in Ref. [11], respectively, and the length scale L of the lattice is assumed to be far larger than r_c . For the two-dimensional triangular lattice

of rod-like nuclei, the mean square of the displacement vector \mathbf{v} of cylinders in a plane perpendicular to their elongated direction is expressed as (Eq. (37) in Ref. [11])

$$\langle |\mathbf{v}|^2 \rangle \simeq \frac{k_B T}{(B + 2C)\sqrt{\pi\lambda a}}, \quad (16)$$

where $\lambda = \sqrt{2K_3/(B + 2C)}$, B , C and K_3 are the elastic constants given by Eqs. (31), (34) and (35) in Ref. [11], respectively, $a = (2\pi/\sqrt{3})^{1/2}r_c$ is the lattice constant for hexagonal cells, and the linear dimension of the lattice in the plane including \mathbf{v} is assumed to be much larger than r_c and to be much smaller than the length of the nuclei. It is important to notice that all the elastic constants, derived by Pethick and Potekhin [14] from the calculations of the electrostatic and interfacial energy increase due to the nuclear deformation, are proportional to the electrostatic energy density, w_{C+L} , given by Eq. (8) in Ref. [11]. Since w_{C+L} in turn behaves as $\propto x^2$, the non-spherical nuclei in supernova cores are more difficult to deform than those in neutron star crusts. As was noted in [11] concerning the crossover temperature T_0 from the quantum-fluctuation to the thermal-fluctuation regime, expressions (15) and (16) hold for $T \gtrsim T_0$ but underestimate the displacements for $T \lesssim T_0$. In the case of supernova matter considered here, T_0 can be roughly estimated to be of order 10^7 K for planar nuclei and of order 10^9 K for cylindrical nuclei.

Let us then ask how large the root-mean-square displacement $\sqrt{\langle |\mathbf{v}|^2 \rangle}$ of a planar or cylindrical nucleus is relative to the shortest distance, $a/2 - r_N$, between the surface of the nucleus in its equilibrium position and the boundary of the cell containing it. The ratio of these two lengths for the planar (cylindrical) nucleus has been plotted in Fig. 8 (9) at $T = 10$ MeV and $L = 10$ km, appropriate to the subnuclear density regime inside

supernova cores; the L dependence of the displacement, which is logarithmic, makes little differences. We can find from these figures the dominance of the relative displacement of the planar nucleus over that of the cylindrical nucleus, yielded by the logarithmic factor appearing in Eq. (15), as well as the suppression of the relative displacements by E_{surf} , which were obtained also for neutron star crusts (see Figs. 7 and 8 in Ref. [11]). This E_{surf} dependence then communicates with the suppression of the relative displacements by Y_L as exhibited in Figs. 8 and 9 via the relation between E_{surf} and Y_L shown in Fig. 1. In examining the competition between the influences of temperature and of elasticity as pointed out in Section 1, it is noteworthy that the relative displacements thus obtained are larger than those obtained for neutron star crusts by less than a factor of ten. This is because the influence of the difference in the typical temperature by two orders-of-magnitude surpasses that of the above-mentioned difference in the elasticity of the nucleus. In case we set the melting condition as $\sqrt{\langle |\mathbf{v}|^2 \rangle} = a/2 - r_N$, the enhanced relative displacements in supernova cores do not modify our previous conclusion [11] obtained for neutron star crusts that the triangular lattice of rod-like nuclei is stable against thermal fluctuations for our typical nuclear model, but change the conclusion about the layered lattice of slab-like nuclei from its marginal instability [11] depending on the nuclear models to its instability almost independent of them. Given uncertainties in the temperature profile of the core, it is useful to estimate the critical temperature T_c at which the relative displacements become unity; the results for T_c have been plotted in Figs. 10 and 11 for the layered lattice and the triangular lattice, respectively.

6 Conclusion

The dependence on the lepton fraction Y_L of the phase diagrams associated with the changes in the nuclear shape has been studied for zero-temperature supernova matter at subnuclear densities. We have found that with increasing Y_L , the density region occupied by the “pasta” phases, i.e., the phases with non-spherical nuclei and with bubbles, becomes larger. Despite the considerable increase in the lepton fraction from neutron star matter, leading to enhancement of the proton fraction in the nuclear matter region and suppression of the density of the dripped neutron gas, not only the sequence of the nuclear shape (sphere \rightarrow cylinder \rightarrow slab \rightarrow uniform with increasing density) obtained for the typical nuclear model but also the effectiveness of thermal fluctuations at the dissolution of slab-like nuclei has been shown to be analogous to the case of neutron star matter.

The actual presence of nuclear “pasta” in supernova cores depends on how the uncertain properties of bulk nuclear matter having a proton fraction of order 0.3 affect the stability of the “pasta” and on whether or not the time needed to form the “pasta” is small compared with the time scale of stellar collapse. If future work about these questions were in favor of the occurrence of the “pasta”, it would be significant to calculate the finite-temperature equation of state and neutrino transport in the presence of the “pasta” phases and to incorporate them into a supernova simulation with a neutrino radiation hydrodynamics code. This would clarify the influence of the “pasta” on the lepton fraction at the onset of the neutrino trapping.

Acknowledgements

This work was supported in part by Grants-in-Aid for Scientific Research provided by the Ministry of Education, Science and Culture of Japan through Research Grant No. 07CE2002 and No. 10-03687.

References

- [1] H.A. Bethe, Rev. Mod. Phys. 62 (1990) 801.
- [2] H. Suzuki, in *Physics and Astrophysics of Neutrinos*, eds. M. Fukugita and A. Suzuki (Springer, Tokyo, 1994), p. 763.
- [3] D.Z. Freedman, Phys. Rev. D9 (1974) 1389.
- [4] K. Sato, Prog. Theor. Phys. 53 (1975) 595; Prog. Theor. Phys. 54 (1975) 1325.
- [5] D.G. Ravenhall, C.J. Pethick and J.R. Wilson, Phys. Rev. Lett. 50 (1983) 2066.
- [6] M. Hashimoto, H. Seki and M. Yamada, Prog. Theor. Phys. 71 (1984) 320.
- [7] M. Lassaut, H. Flocard, P. Bonche, P.H. Heenen and E. Suraud, Astron. Astrophys. 183 (1987) L3.
- [8] A. Mezzacappa, M. Liebendörfer, O.E.B. Messer, W.R. Hix, F.-K. Thielemann and S.W. Bruenn, astro-ph/0005366.
- [9] C.J. Horowitz, Phys. Rev. D55 (1997) 4577.
- [10] S.W. Bruenn and A. Mezzacappa, Phys. Rev. D56 (1997) 7529.
- [11] G. Watanabe, K. Iida and K. Sato, astro-ph/0001273 (to be published in Nucl. Phys. A).
- [12] K. Oyamatsu, I. Tanihata, Y. Sugahara, K. Sumiyoshi and H. Toki, Nucl. Phys. A634 (1998) 3.

- [13] G. Baym, H.A. Bethe and C.J. Pethick, Nucl. Phys. A175 (1971) 225.
- [14] C.J. Pethick and A.Y. Potekhin, Phys. Lett. B427 (1998) 7.
- [15] D.G. Ravenhall, C.D. Bennett and C.J. Pethick, Phys. Rev. Lett. 28 (1972) 978.
- [16] J. Arponen, Nucl. Phys. A191 (1972) 257.
- [17] K. Kolehmainen, M. Prakash, J.M. Lattimer and J.R. Treiner, Nucl. Phys. A439 (1985) 535.
- [18] R. Ogasawara and K. Sato, Prog. Theor. Phys. 68 (1982) 222.

Fig. 1. The surface energy per unit area (the surface tension) as a function of x . The thick lines are the present results obtained from Eq. (6) for $C_1 = 400 \text{ MeV fm}^2$, $C_2 = 0.01, 0.1, 0.5, 1.0, 2.5$ and $Y_L = 0.2, 0.3, 0.4$. The solid curve is the RBP result from their HF calculation [15], and the dotted curve is the BBP result [13]. The cross denotes the value adopted by Ravenhall et al. [5].

Fig. 2. Zero-temperature phase diagrams on the n_b versus C_2 plane, evaluated for $Y_L = 0.3$ and $C_1 = 300, 400, 600 \text{ MeV fm}^2$.

Fig. 3. Zero-temperature phase diagrams on the n_b versus C_2 plane, evaluated for $Y_L = 0.2, 0.25, 0.3, 0.4$ and $C_1 = 400 \text{ MeV fm}^2$.

Fig. 4. Energy per nucleon relative to that of uniform matter calculated for $Y_L = 0.3$, $C_1 = 400 \text{ MeV fm}^2$ and $C_2 = 1.0$ as a function of baryon density n_b . The symbols SP, C, S, CH and SPH stand for sphere, cylinder, slab, cylindrical hole and spherical hole, respectively.

Fig. 5. Energy per nucleon of the phase with spherical bubbles relative to that with slab-like nuclei, calculated for $Y_L = 0.3$, $C_1 = 400 \text{ MeV fm}^2$ and $C_2 = 1.0$ as a function of baryon density n_b . The absolute value of the curvature energy per nucleon of the phase with spherical bubbles is also evaluated for the curvature thermodynamic potential per unit length $\omega_c = 0.1, 0.2, 0.5 \text{ MeV fm}^{-1}$.

Fig. 6. Size of a nucleus or bubble, r_N , and of a Wigner-Seitz cell, r_c , calculated for $Y_L = 0.3$, $C_1 = 400 \text{ MeV fm}^2$ and $C_2 = 0.01, 1.0, 2.5$ as a function of baryon density n_b . The symbols SP, C, S, CH and SPH stand for sphere, cylinder, slab, cylindrical hole and spherical hole, respectively.

Fig. 7. The neutron densities obtained for $Y_L = 0.3$, $C_1 = 400 \text{ MeV fm}^2$ and $C_2 = 0.01, 0.1, 1.0, 2.5$ as a function of baryon density n_b . The lines classified by $[n(1-x)]_N$ and n_n represent the neutron densities in the nuclear matter region and in the neutron gas region for the phases with nuclei, respectively. The lines classified by $[n(1-x)]_{\text{uni}}$ denote the neutron densities in uniform nuclear matter.

Fig. 8. The root-mean-square displacement of a planar nucleus at $k_B T = 10 \text{ MeV}$, divided by the shortest distance between the surface of the nucleus in its equilibrium position and the boundary of the cell containing it. The curves are obtained for $C_1 = 400 \text{ MeV fm}^2$ and for various sets of Y_L and C_2 as a function of baryon density n_b . The thick curves lying between the two vertical lines are the results in the density region in which the phase with planar nuclei is energetically stable.

Fig. 9. The root-mean-square displacement of a cylindrical nucleus at $k_B T = 10 \text{ MeV}$, divided by the distance between the surface of the nucleus in its equilibrium position and the boundary of the cell containing it. The curves are obtained for $C_1 = 400 \text{ MeV fm}^2$ and for various sets of Y_L and C_2 as a function of baryon density n_b . The thick curves lying between the two vertical lines are the results in the density region in which the phase with cylindrical nuclei is energetically stable.

Fig. 10. The critical temperature T_c for the phase with planar nuclei as a function of baryon density n_b . The thick curves lying between the two vertical lines are the results in the density region in which the phase with planar nuclei is energetically stable. C_1 is taken to be 400 MeV fm^2 .

Fig. 11. The critical temperature T_c for the phase with cylindrical nuclei as a function of baryon density n_b . The thick curves lying between the two vertical lines are the results in the density region in which the phase with cylindrical nuclei is energetically stable. C_1 is taken to be 400 MeV fm².

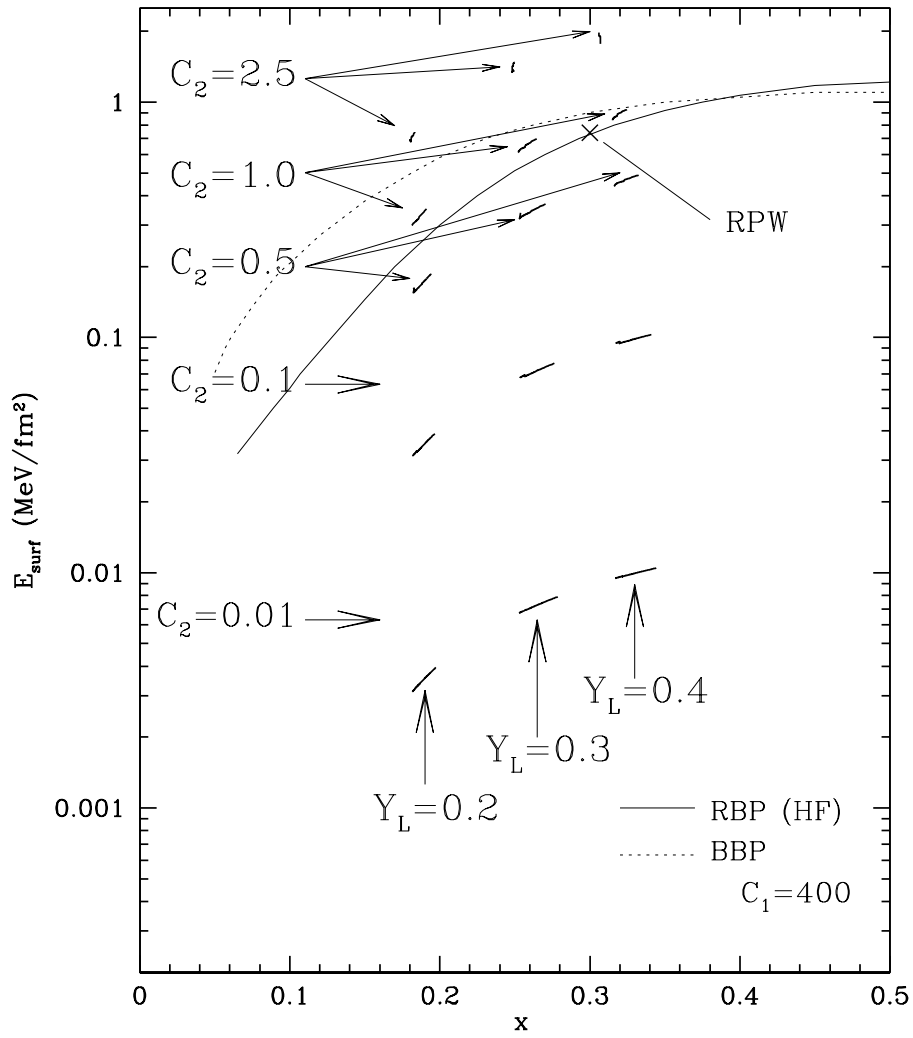


Figure 1:

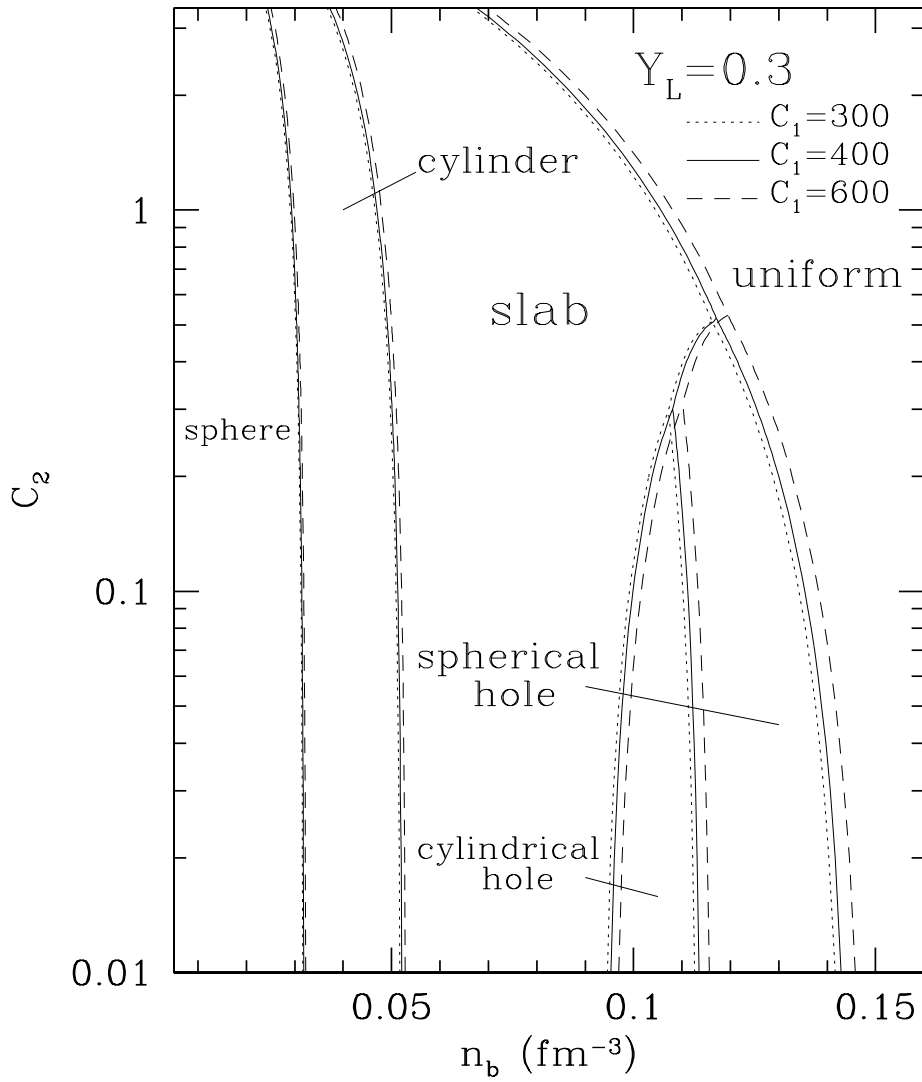


Figure 2:

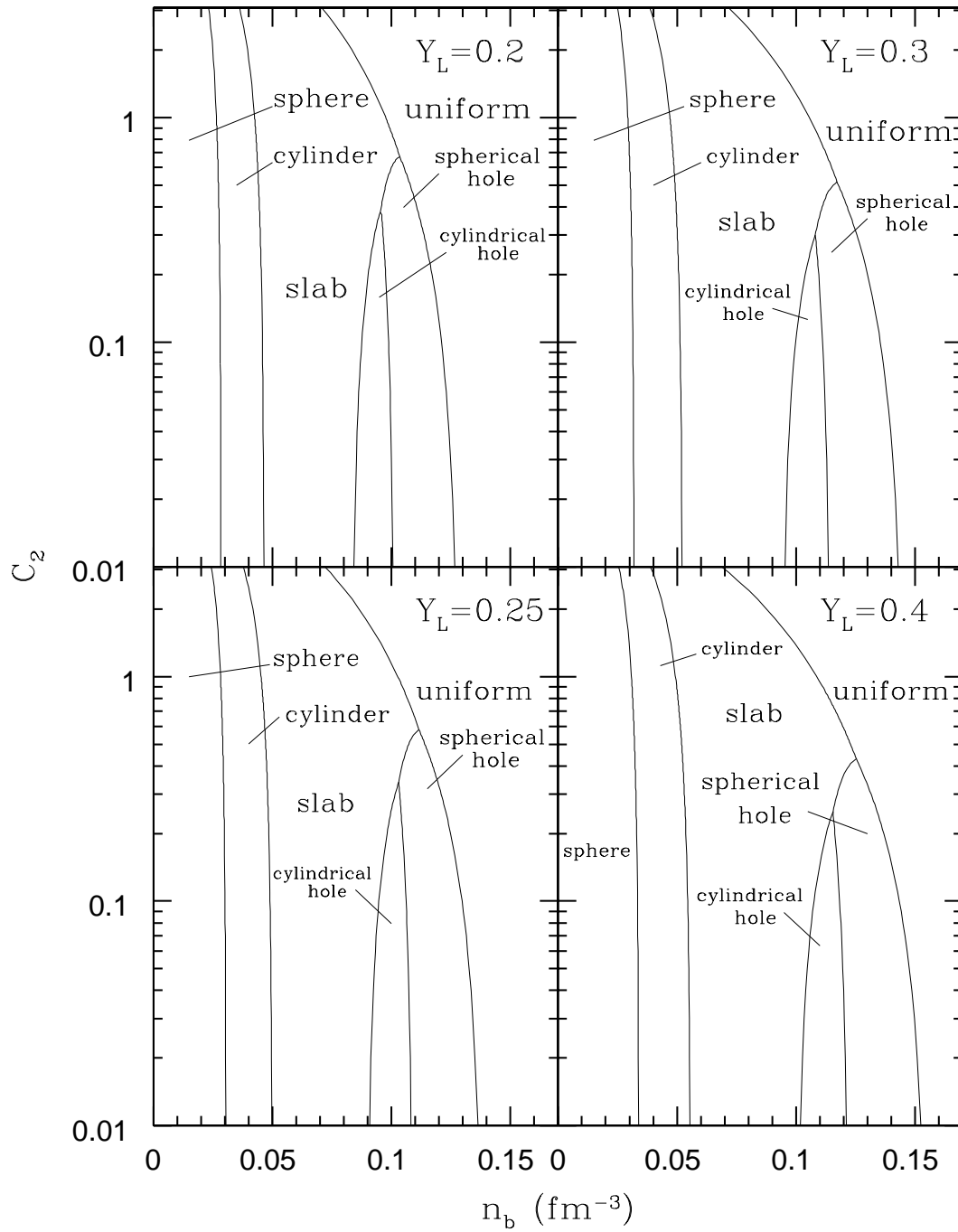


Figure 3:

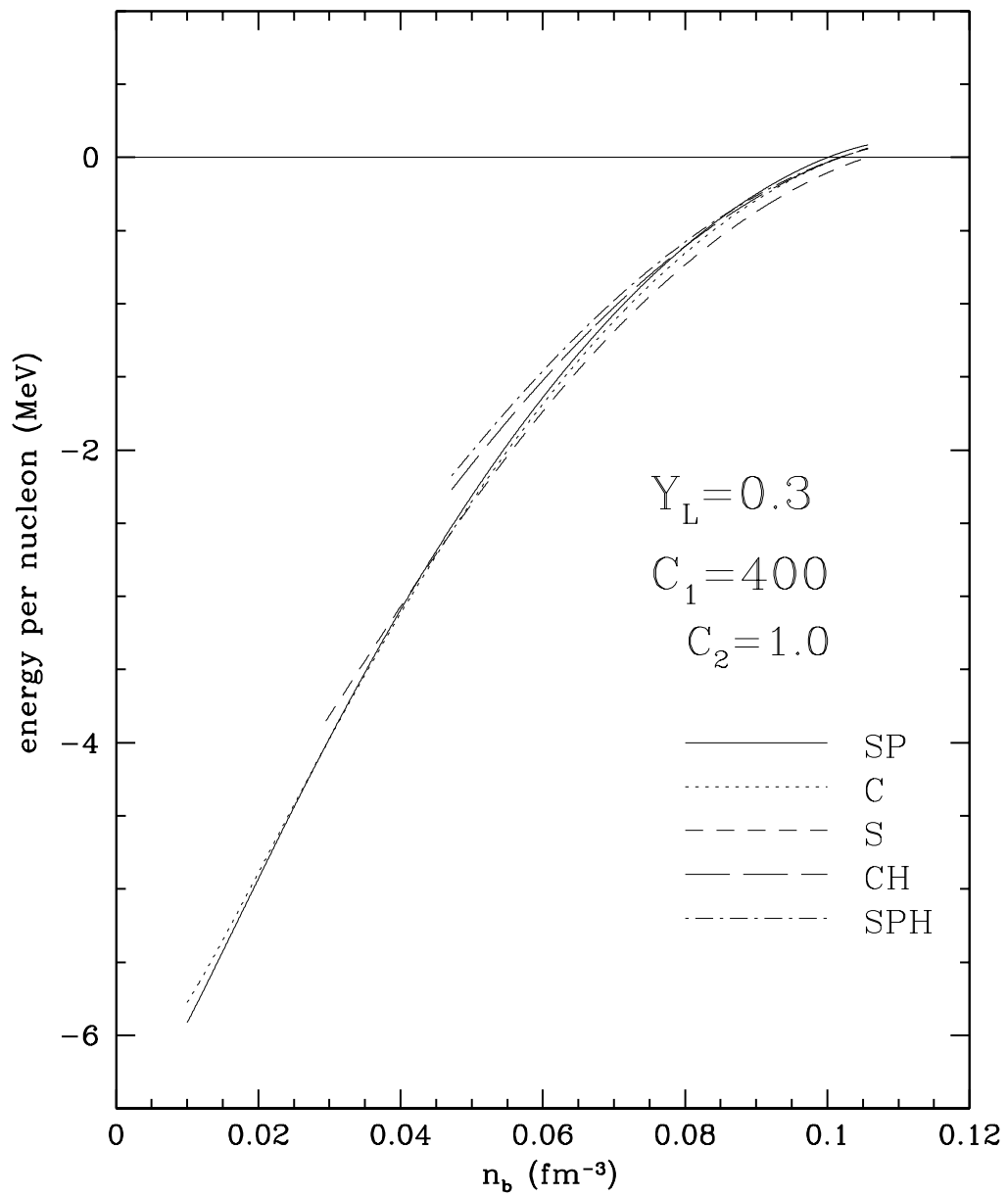


Figure 4:
30

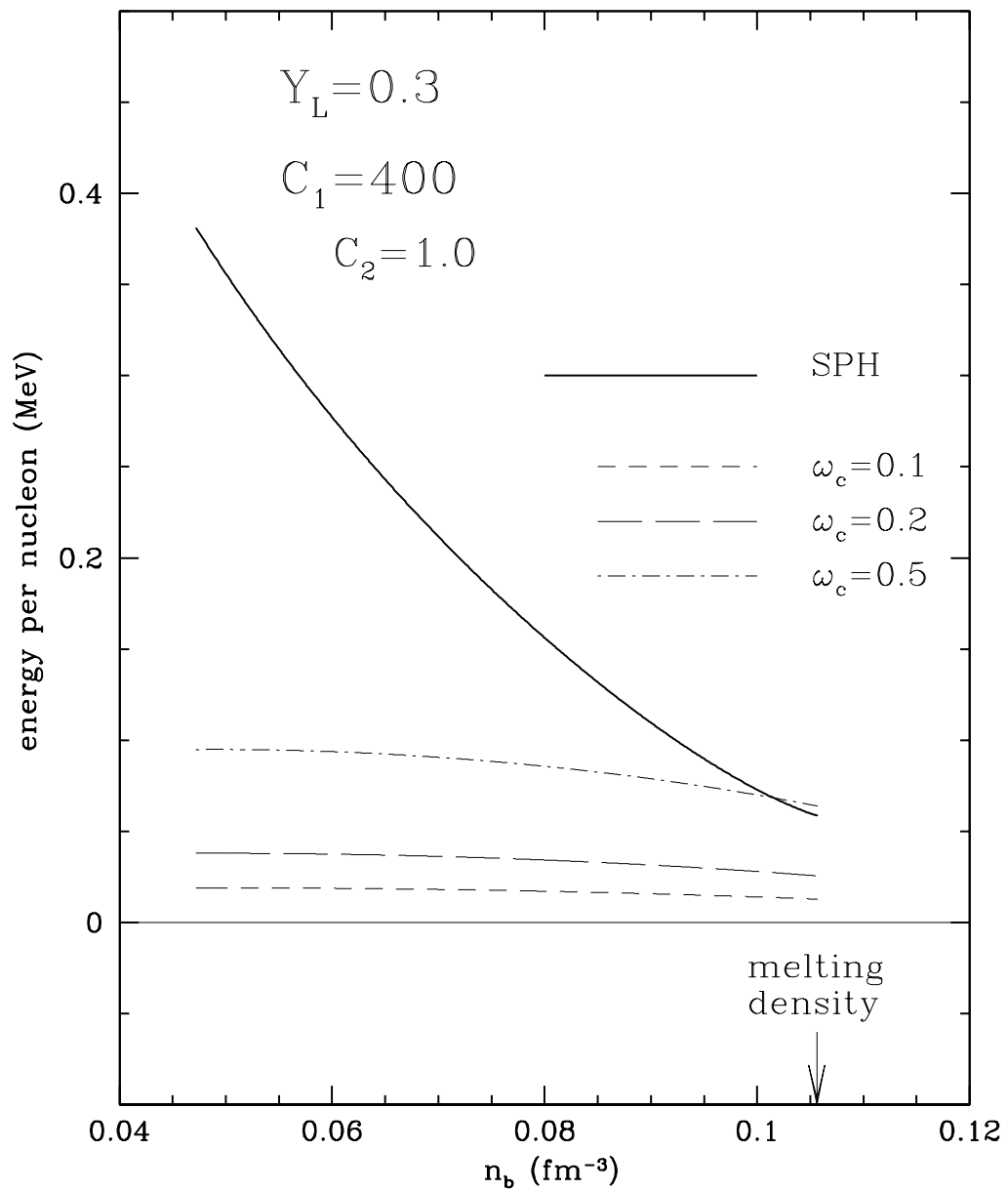


Figure 5:

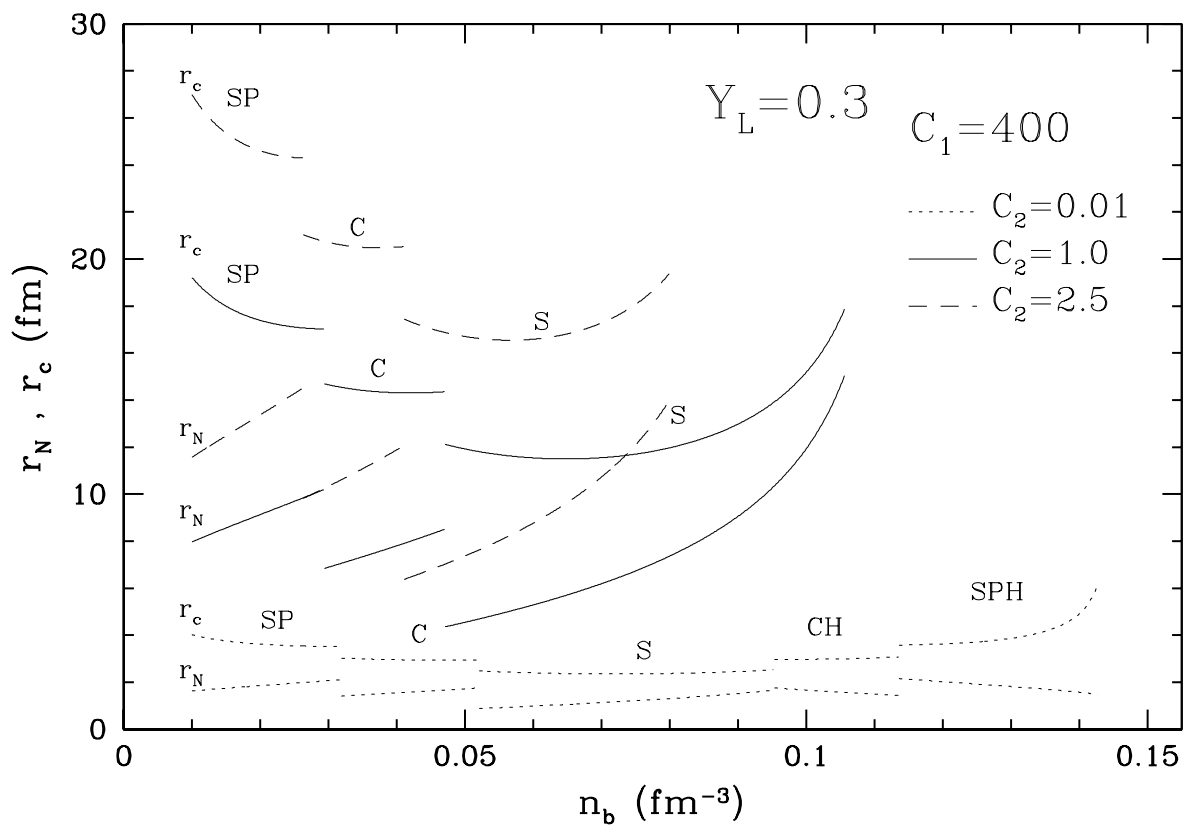


Figure 6:

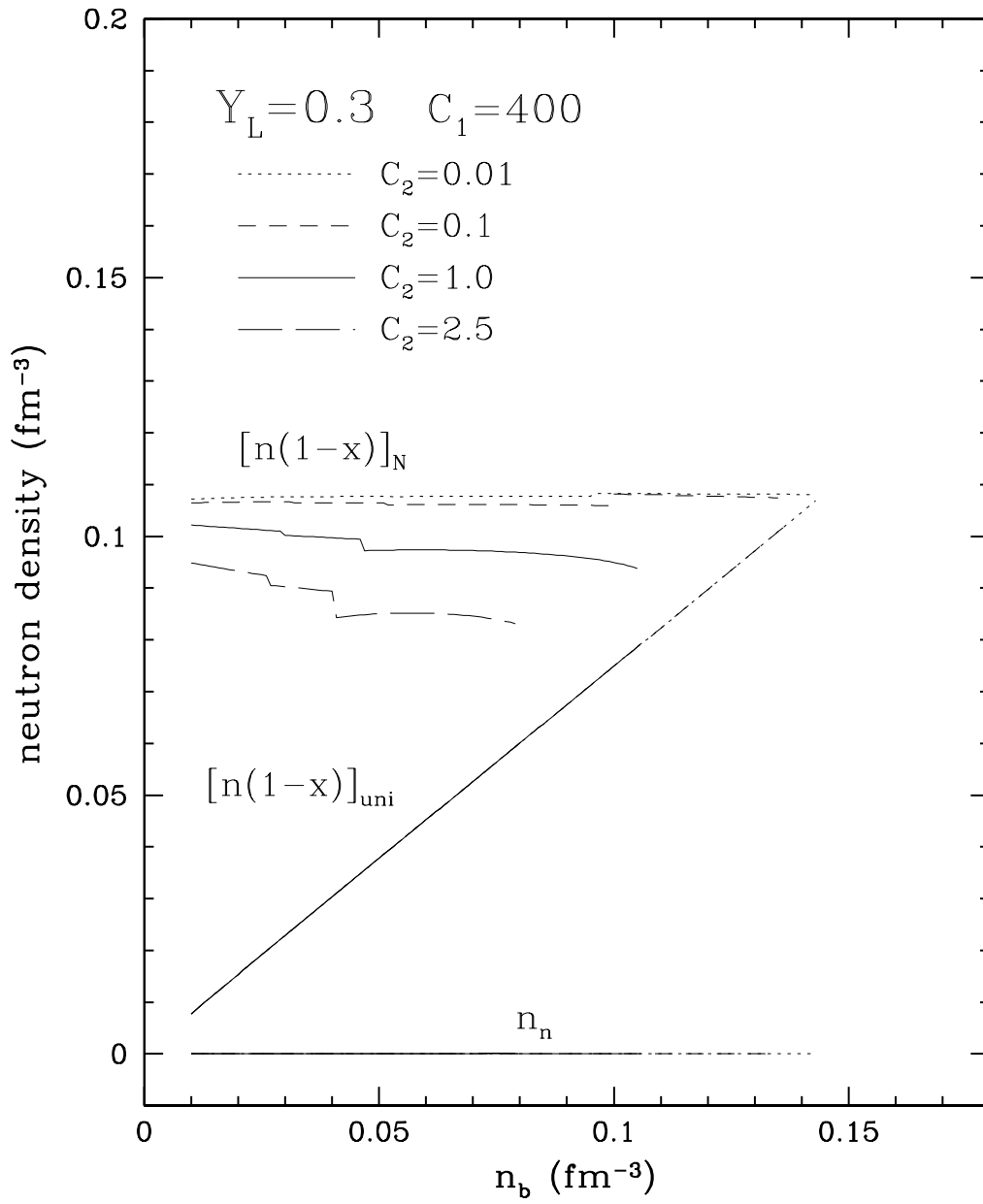


Figure 7:

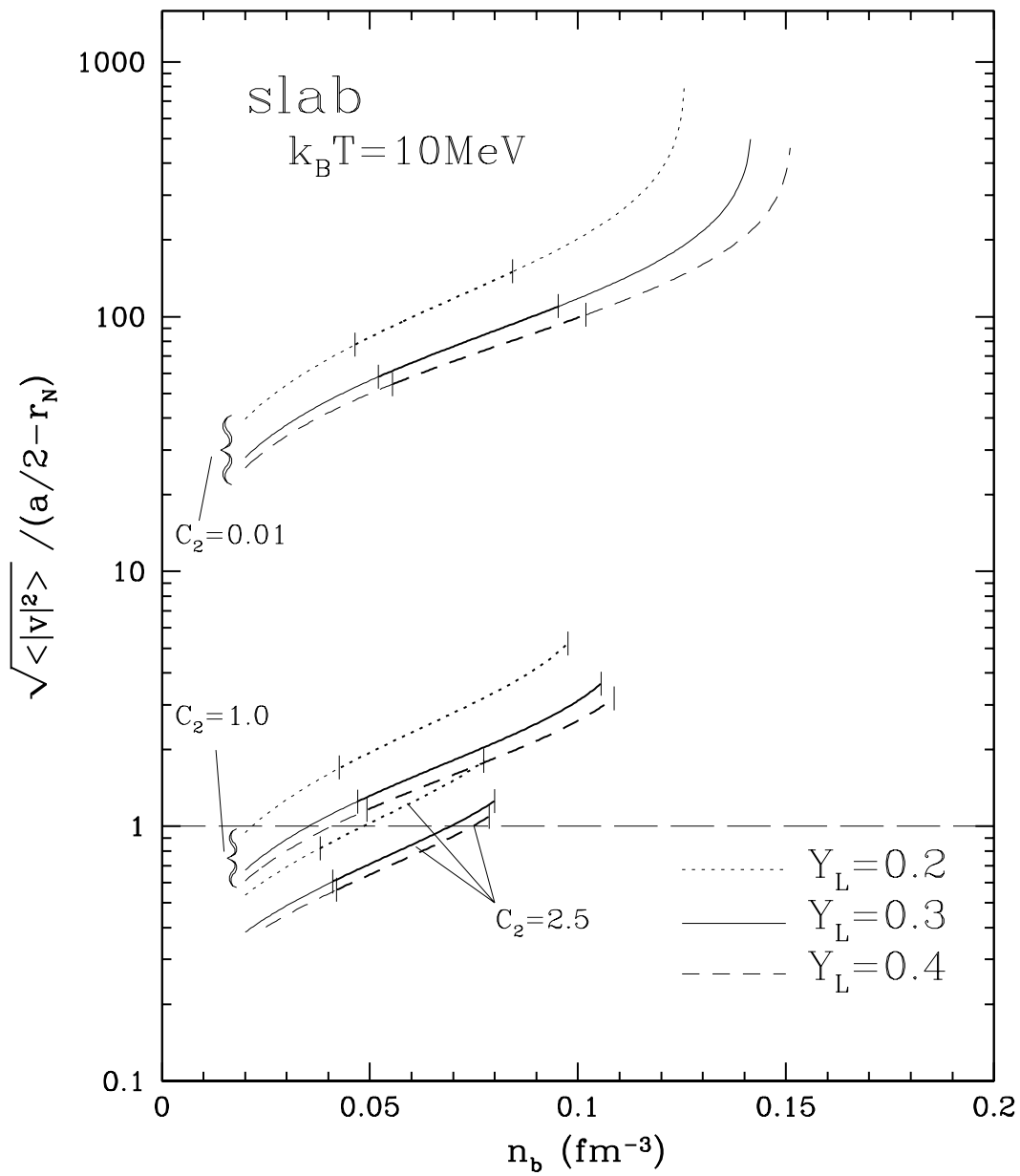


Figure 8:

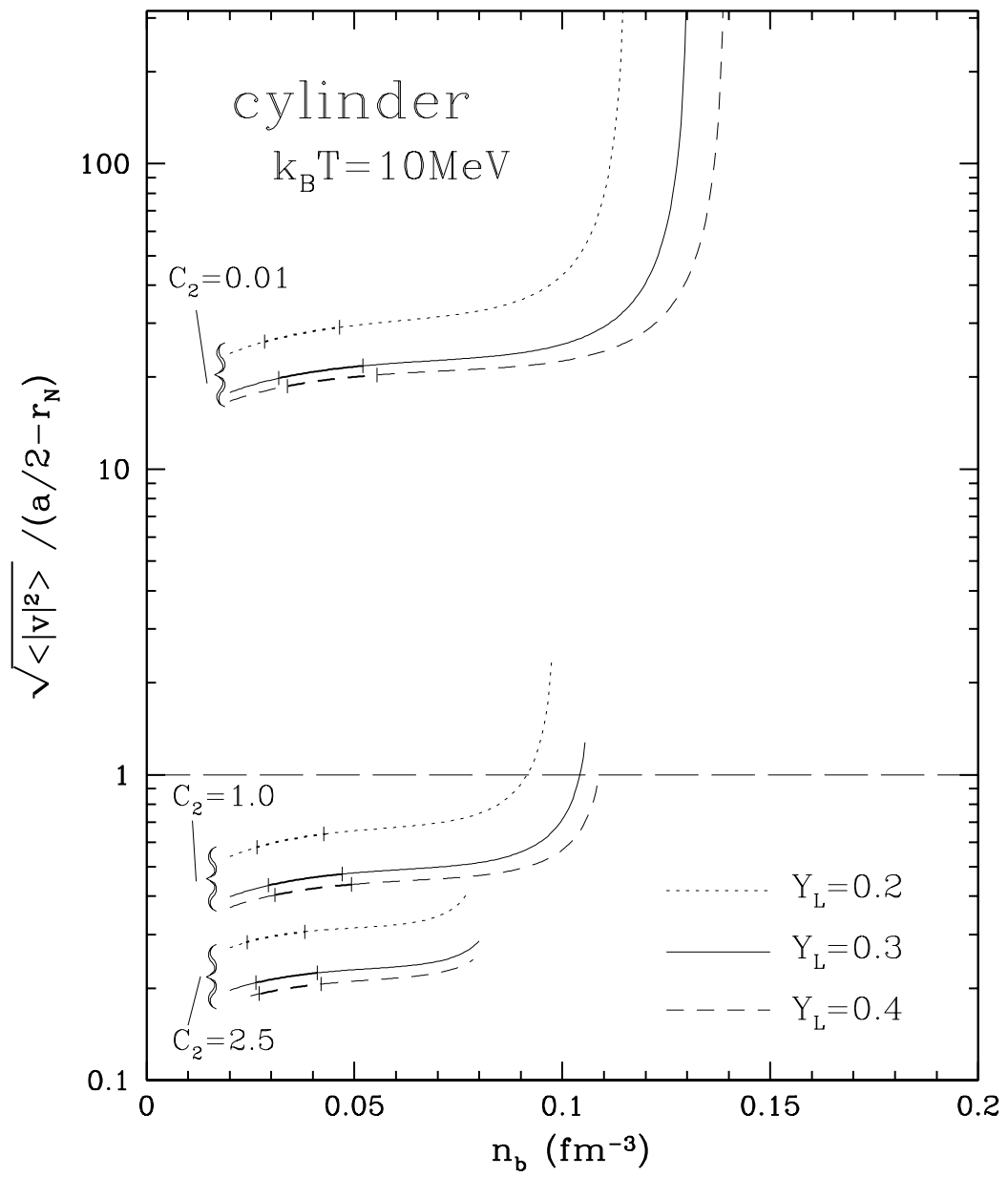


Figure 9:

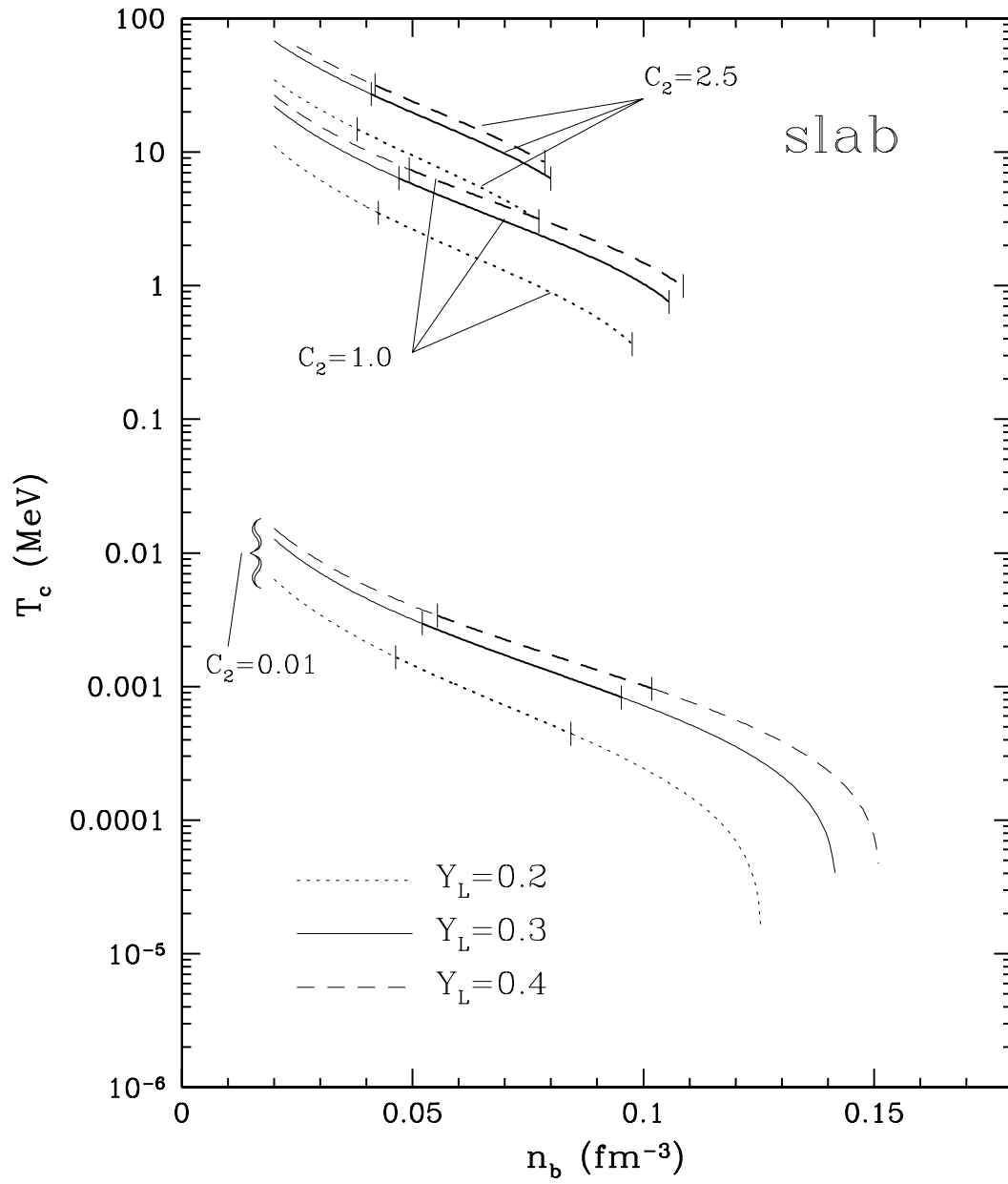


Figure 10:
36

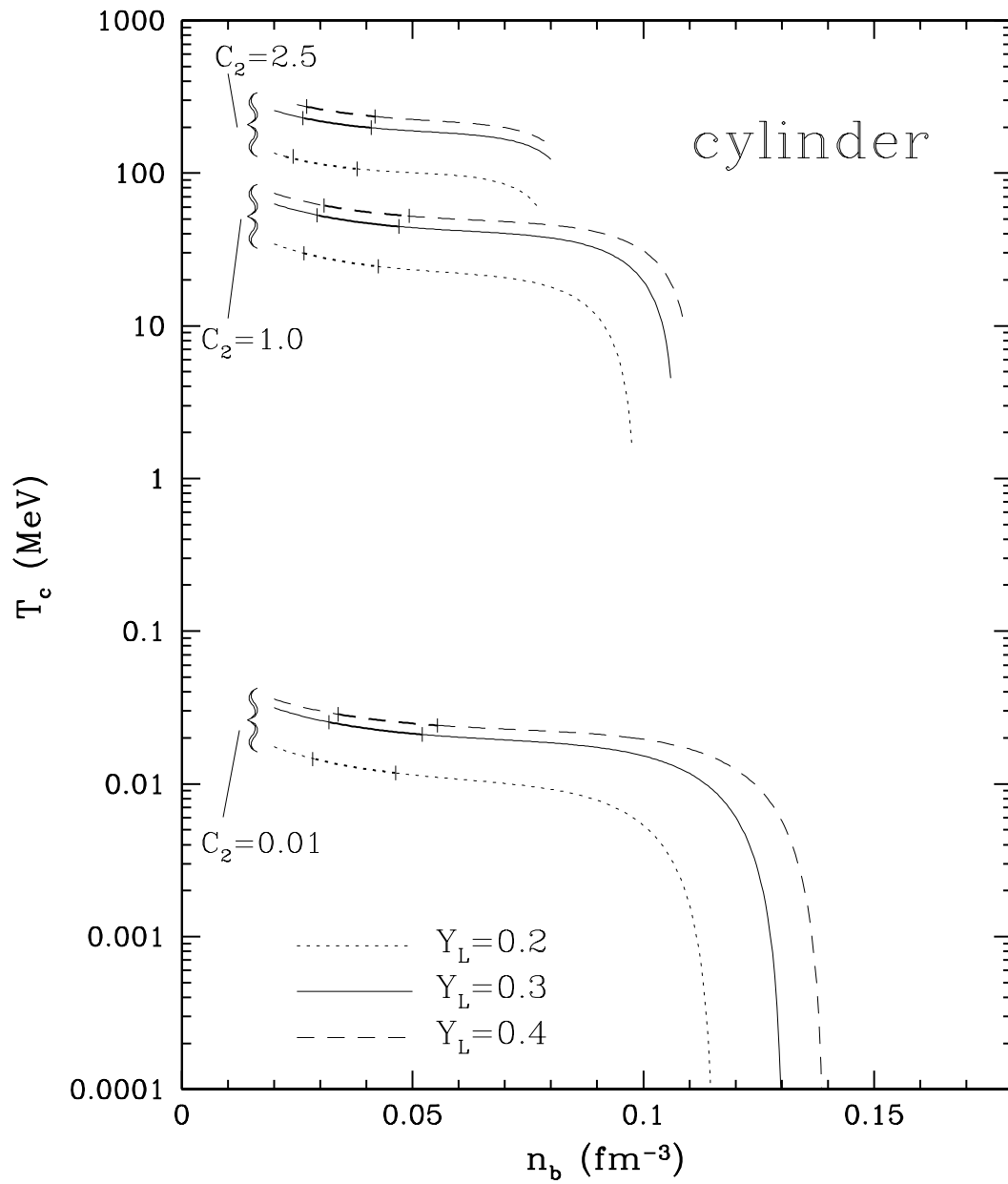


Figure 11:
37